International Journal of Engineering Inventions
e-ISSN: 2278-7461, p-ISSN: 2319-6491
Volume 12, Issue 7 [July. 2023] PP: 64-75

Study of the structural characteristics and two-phase model in glass and liquid Al_2O_3 using molecular dynamics simulation

Giap Thi Thuy Trang, Phan Dinh Quang and Pham Huu Kien
Department of Physics, Thainguyen University of Education, No. 20 Luong Ngoc Quyen, Thai Nguyen, VIETNAM
E-mail: tranggtt@tnue.edu.vn; kienph80@tnue.edu.vn

Abstract:
The structural characteristics and two-phase model in glass and liquid Al_2O_3 under compression and temperature were successfully investigated by molecular dynamics simulation. The structural characteristics of samples are examined through AlO_x units, the bond angle and length distributions, order parameters, and the visualization technique. The result shows that the structural organization of glass and liquid Al_2O_3 is built mainly by AlO_x (x = 3, 4, 5, 6, 7) units that are linked to each other via common O atoms. With increasing pressure, the fraction of AlO_x units significantly varies, but partial bond angle and length distributions of AlO_x units are identical for all the different pressures. We suggest that the density of constructed samples may be expressed by a linear function of a fraction of AlO_x units. In addition, the distribution of AlO_x units in network structure is not uniform but tends to form clusters contained AlO_x units. During a moderately long time, the liquid comprises the two phases that consist of separate low-density, and high-density phases. The size of these phases significantly depends on compression. This allows us to suggest a simple correlation between the diffusion coefficients and the characteristics of two phases. Our work is expected to contribute a simple way to determine the diffusion coefficients as well as the density of oxide systems.
Keywords: *Simulation, structure, cluster, phase, low-density, high-density*

Date of Submission: 28-06-2023 Date of acceptance: 08-07-2023

I. Introduction

Aluminum Al_2O_3 is very important ceramic material that has many technological applications such as in high-temperature crucibles, cements, abrasives, ceramics, and get famous solid-phase structures [1-5]. Therefore, knowledge of the polyamorphism of liquid and glass Al_2O_3 is essential and in fact, their structural and dynamics features have been investigated in detail by a number of researchers, e.g. [6-11].

As we well known, liquid and glass Al_2O_3 is a network-forming, whose structure consists of a three-dimensional network of oxygen-shared AlO_4 tetrahedrons. At ambient pressure, the Al-O bond length is close to 1.72 ± 0.02 Å. The average tetrahedral angle shows a maximum at $141^o \pm 5^o$. In addition, the strong directional bonds and high degree of intermediate range order are found to persist in the liquid and glass phase as reported in refs. [12-18]. Many experimental studies of Al_2O_3 glass confirmed that with increasing pressure, the liquid and glass undergoes a gradual transformation from four- to six-fold coordination, resulting in a network of AlO_6 octahedrons as showed in refs. [19-21].

So far, simulation techniques also provide details about the microstructural properties, as well as the phase transformation at atomic levels. The molecular dynamics (MD) and *ab*-initio simulation with applied effective potentials [7,16,18] reproduces well the structural factors obtained experimentally, but the bond angle distribution is rather broad to be compatible with experimental data. By using MD simulation, the polyamorphism and the existence of many glass and liquid states with different pressure have explained based on the two-phase model as reported in refs. [22,23]. In addition, the structure characteristics of glass (liquid) Al_2O_3 (GeO_2, H_2O, B_2O_3, Al_2O_3, TiO_2, Y_2O_3-Al_2O_3 etc.) is investigated through two glass (liquid) phases, namely low-density and high-density phases. The coexistence of two phases with the different fraction leads to the different densities of the same composition. However, the atomic arrangement in space regions between AlO_x units is poorly defined in these works.

About dynamics properties of oxide systems, as shown in ref. [24], the behavior of sell-diffusion coefficient is consistent with crossover from strong to fragile liquid behavior with increasing temperature and pressure. Both O and Si self-diffusion coefficients vary anomalously at 4000 K. Jiang et al. [25] revealed that in SiO-CaO-MgO-Al_2O_3 systems, the diffusion coefficient order of ions from large to small is Mg^{2+}, Ca^{2+}, Al^{3+},

O^{2-}, Si^{4+}. The total self-diffusion coefficient of all atoms showed an increasing trend, which reflects that the viscosity became lower. Guo et al. [26] shown that in the KF-NaF-AlF_3-Al_2O_3 system, the diffusion ability of various atoms is as follows Na > K > F > O > Al. With the increasing concentration of Al_2O_3, the ionic conductivity decreases but the viscosity increases gradually, which is consistent with the changing rule of ionic structure. Gao et al. [27] found that with increasing the CaO/Na_2O ratio in SiO_2-Al_2O_3-CaO-Na_2O system, the atomic diffusivity decreases. Feng et al. [28] showed that the order of the diffusion ability of ions from small to large is O, Si, Al, F, and Na. The addition of SiO_2 into Na_3AlF_6-Al_2O_3 molten salt causes an increase of the viscosity and a decrease of ionic conductivity. To clarify the dynamics heterogeneity (DH) a set of most mobile atoms are selected, and the clusters where those atoms reside are determined. In the case when DH occurs, the average size of clusters of most mobile atoms is larger than that from random statistics [29]. The multipoint correlation functions and Van Hove self-correlation function are also used to identify DH [30]. Although previous simulations provided evidences of DH, many aspects of this phenomenon remain unclear.

Therefore, in this paper, we focus on studying the structural characteristics and indicating the existence of two phases with high- and low-density of liquid and glass Al_2O_3. The properties of Al_2O_3 are inferred from simulated models by the bond length, bond-angle distribution, coordination number, and the visualization technique.

II. Computational method

MD simulation has been done in the cubic box with periodic boundary condition for 3000 atoms (1200 Al and 1800 O atoms). We use the Born-Mayer type pair potential to construct the Al_2O_3 glass models. The form of the potential is

$$U_{ij}(r_{ij}) = \frac{q_i q_j}{r_{ij}} + B_{ij}\exp\left(-\frac{r_{ij}}{R_{ij}}\right) \qquad (1)$$

The terms in Eq. (1) represent Coulomb and repulsion energy, respectively. Here r_{ij} is interatomic distance between i^{th} and j^{th} ions; q_i and q_j are the charges of i^{th} and j^{th} ions; B_{ij} and R_{ij} are parameters accounting the repulsion of the ions shells which are listed in the Table 1. The long-range Coulomb interactions are calculated with the standard Ewald simulation method. The equations of motion are integrated with Verlet algorithm, here we use a time step 0.4 fs.

Table 1. The potential parameters for Al_2O_3 glass, as seen in refs. [6,7,18]

Pairs	B_{ij} (eV)	R_{ij} (Å^{-1})	q_i, q_j (eC)
Al-Al	0.0	0.0	q_{Al} = +3.0
Al-O	1479.86	3.4483	q_O = -2.0
O-O	1500	3.4483	-

This initial configuration is heated to 6000 K at ambient pressure and relaxed over 5×10^4 time steps. Then, the model is cooled to 3000, 1000 and final 300 K, at zero pressure during 3×10^4 time steps. Next, system is allowed to reach equilibrium for over 10^5 time steps. With this well-equilibrated model at the temperature of 300 and 3000 K, we prepared 12 models with pressure of 5, 10, 15, 20, 25, 30 GPa, corresponding with the temperature of 300 and 3000 K. After that the models has been relaxed in NVE ensemble (the constant volume and energy) for 5×10^4 time steps, to reach the equilibrium. The network structure is studied via basic AlO_x units. The cutoff distance r_{cutoff} used equals 2.4 Å which is chosen from first minimum of the PRDF $g_{Al\text{-}O}(r)$.

In this work, the total XRSSF $S_N(r)$ is calculated from pair XRSSFs $S_{Al\text{-}Al}(r)$, $S_{Al\text{-}O}(r)$, $S_{O\text{-}O}(r)$. The total XRSSF is defined by

$$S_N(q) = \frac{\sum_{\alpha\beta}^{n} C_\alpha f_\alpha C_\beta f_\beta S_{\alpha\beta}(q)}{\left[\sum_\alpha C_\alpha f_\alpha\right]^2} \qquad (2)$$

Where q is the scattering vector, n is the total number of the element types in the sample; C_α, C_β are the number fraction of species α, β; f_α, f_β are the corresponding X-ray scattering length of Al and O atoms. We take f_{Al} = 3.654×10^{-14}, f_O= 2.249×10^{-14}m as used in refs. [15,19]. The $S_{\alpha\beta}(r)$ term is the pair XRSSFs, it is examined based on the pair radial distribution function, $g_{\alpha\beta}(r)$ using the Fourier transformation

$$S_{\alpha\beta}(q) = 1 + \rho_\beta \int_0^R 4\pi r^2 \left[g_{\alpha\beta}(\mathrm{r}) - 1\right] \frac{\sin qr}{qr} \frac{\sin(\pi\,\mathrm{r}/\,\mathrm{R})}{\pi\,\mathrm{r}/\,\mathrm{R}} dr \qquad (3)$$

where ρ_β represents the average number density of β atom, the cut-off length R is selected to be half the distance of the simulation box, and r is the inter-atomic length [12,15].

III. Results and discussion

Firstly, to evaluate the reliability of our model, we compare the total X-ray scattering structure factors (XRSSF) as obtained from the present simulation with the experimental and other simulation data reported by Lamparter et al. [31], Landron et al. [14], and Gutierrez et al. [15, 19], Vashishta [32] respectively. As shown in Figure 1, there is good agreement between the experimental and simulated XRSSFs $S_N(q)$ for Al_2O_3 glass. In the case of Al_2O_3 liquid, the agreement with the experiment for $q \geq 3.0$ Å^{-1} is very good in terms of the shape, position, and amplitude of the peaks. For low q, although the simulation results do not fit completely with experimental curves, it is clear that they resemble fairly well the 'sub-peak' which is present at $q \sim 2.1$ Å^{-1}. In addition, Table 1 shows some structural characteristics of Al_2O_3 liquid and glass. In our constructed samples, good agreement is observed between the experimental and simulated data except for the coordination number $Z_{O\text{-}O}$ which may relate to the choice of length cut-off for O-O bond. With increasing pressure, the bond length $r_{Al\text{-}Al}$ and $r_{O\text{-}O}$ decrease gradually, meanwhile the bond length $r_{Al\text{-}O}$, bond angles $\theta_{O\text{-}Al\text{-}O}$, $\theta_{Al\text{-}O\text{-}Al}$ are slightly changed, respectively.

Figure 2 shows the total XRSSF of Al_2O_3 liquid and glasses at different pressures. As well known, the low q-parts are related to intermediate-range order (IRO), while the first (main) peak of the XRSSF distributed from nearest-neighbor Al-Al, Al-O, and O-O connections. In both cases, the first peak of the XRSSF is located at 2.1 Å^{-1} (at ambient pressure), which shifts to the right and the height of the XRSSF decreases with increasing pressure, this peak reaches 2.4 Å^{-1} (at the pressure of 30 GPa). For Al_2O_3 liquid, as seen, the second sub-peak appears at around 5 GPa, which relates to the phase transition point of the liquid. The main second peak of XRSSF is located at 4.7 Å^{-1} (at ambient pressure), which shifts to the left with increasing pressure, it reaches 4.4Å^{-1} (at the pressure of 30 GPa). Unlike Al_2O_3 liquid, the second sub-peak of Al_2O_3 glass appears at around 20 GPa, the main second of XRSSF is located at 4.7 Å^{-1} which is not dependent on pressure. Therefore, it can be concluded that the phase transition point for glass at pressure is higher than that for liquid. Under compression, the IRO of liquid significantly changes, in contrast, for glass lightly changes.

Figure 3 presents the pressure dependence of fraction of AlO_x basic units. The fraction of AlO_x basic units is defined as $C_{AlOx} = n_{AlOx}/n_{Al}$; where n_{AlOx}, n_{Al} is the number of AlO_x units and Al atoms, respectively. In both cases, it could be noticed that the fraction of C_{AlO4} monotonously decreases with increasing pressure, while the fraction of C_{AlO6} increases, indicating the transformation from tetrahedral to octahedral network structure. Besides, for Al_2O_3 liquid, the curve for C_{AlO5} intersects with the one for C_{AlO4} and C_{AlO6} at around 12 and 22.5 GPa, respectively, meanwhile, for liquid at round 7.5 and 16 GPa. This means that the phase transition pressure, as well as the phase transition pressure range in liquid is lower (or smaller) than those in glass. This also predicts from the features of the total XRSSF under compression as indicated in Figure 2. Although the fractions of different type basic units vary strongly with increasing pressure, the topology of AlO_x units (x = 4, 5, 6) remain almost constant. According to Figure 2, the structure of Al_2O_3 (liquid or glass) comprises two phases: low-density phase (LD phase) and high-density phase (DH phase) [23,33,34-36]. The network structure of LD phase is built from AlO_4 units. The AlO_4 units connect together via OAl_2 linkages, forming a cluster of AlO_4 units (AlO_4 sub-network). The network structure of HD phase is built from AlO_5, AlO_6, and AlO_7 units, they are connected via OAl_2 and OAl_3 linkages, forming a cluster of AlO_x units (AlO_x sub-network, with x = 5, 6, 7).

The bond angle distribution (BAD) and bond length distribution considered separately for each type of basic unit are presented in Figures 4 and 5. It could be noticed that the BAD and bond length distribution for AlO_4, AlO_5, and AlO_6 is almost independent of pressure and temperature. Only small deviations in the height and position of BAD main peak are seen for AlO_5 unit which may be related to the phase transition process in liquids and glasses. This phenomenon is confirmed that the short-range order (SRO) of Al_2O_3 liquid and glass do not sensitive to pressure and temperature.

To make insights into the phase transition in Al_2O_3 liquid and glass, the order parameter is used, it forms as follows

$$\eta(P) = \frac{n_6 - n_4}{n_6 + n_4} \qquad (4)$$

Where n_4 and n_6 are the total numbers of AlO_4 and AlO_6 units if $\eta(P) = -1$ there are no AlO_6 units in the system and the same if $\eta(P) = 1$ there are no AlO_4 units. Figure 6 shows the curve of the order parameter as a function of pressure. As seen, the curve of the order parameter for liquid and glass increases with increasing pressure, indicating the transformation from tetrahedral to octahedral network structure. It could be noticed that abrupt variation from the AlO_4 to the AlO_6 units has not been observed clearly, which may be due to the

existence of the AlO_5 units in the liquid and glass [37]. This implies that the first or second-order nature of the phase transition in liquid and glass is not found clearly [38,39].

With increasing pressure, there is a gradual transition from the LD phase to HD phase corresponding to the gradual structural transition from tetrahedral to octahedral network structure. In the density-range of 3.07-4.28 g/cm^3, the structure of liquid Al_2O_3 comprises both phases: LD and HD phase. At a definite density, the linkages between AlO_x units consist of both OAl_2 and OAl_3. The AlO_4 units relate to LD phase, and the AlO_5, AlO_6, and AlO_7 units relate to HD phase. As a result, the density of samples can be expressed through fraction of AlO_x units, it has form as follows

$$\rho = C_4\rho_{LD} + (C_5 + C_6 + C_7)\rho_{HD} \qquad (5)$$

where, C_4, C_5, C_6 and C_7 are the fraction of AlO_x (x = 4, 5, 6, 7), respectively, ρ_{LD} and ρ_{HD} are the densities in LD and HD phases. The ρ_{LD} and ρ_{HD} are calculated by fitting function in Eq. (5) with molecular dynamics simulation data, these fitting parameters are ρ_{LD} = 2.54 ± 0.05 and ρ_{HD} = 4.44 ± 0.05 g/cm^3. Therefore, the density of Al_2O_3 glass and liquid is dependent on the fraction of AlO_x units and the arrangement of AlO_x (x = 4, 5, 6, 7) units [40,41]. Figure 7 presents the pressure dependence of density of liquid Al_2O_3 in the pressure range of 0-30 GPa. As seen, the curve of density calculated by Eq. (5) is in good agreement with one of simulation. It confirms the polyamorphism of liquid Al_2O_3 and the power of the two phase model.

To clarify the polyamorphism and the structural phase transformation in the liquid Al_2O_3, the network structure of samples has been visualized. The distribution of AlO_x units (LD and HD phases) in samples is depicted in Figure 8. It could be noticed that the AlO_4 units in the samples are not uniform but it tends toward cluster-forming with LD. On the other hand, the AlO_5 and AlO_6 tend toward cluster-forming with HD. The size of LD and HD clusters significantly depends on pressure. In the low-pressure region (0, 5 GPa), the structure of samples is mainly formed by the LD cluster. With increasing pressure, the size of LD clusters is narrowed; in contrast, the size of HD clusters is expanded. In the high-pressure region (20, 30 GPa), the structure of samples is mainly formed from the LD clusters. At definite pressure, the structure of liquid Al_2O_3 contains both phases, and the sample's density is detected by Eq. (5).

Finally, we focus on dynamics properties of Al_2O_3 liquid. As well know, for liquid, the diffusion coefficient of atoms can be determined via the Einstein equation as following:

$$D_X = \lim_{t\to\infty} \frac{<\Delta r_X(t)^2>}{6t} = \frac{1}{N}\lim_{t\to\infty} \frac{\sum_{i=1}^{N}\left\langle \left[r_{Xi}(t) - r_{Xi}(t)\right]^2 \right\rangle}{6t} \qquad (6)$$

where N is the number total of atoms in a sample, $r_{Xi}(t)$ is the position of i^{th} X-atom at time t. To calculate the diffusion coefficients, each sample is relaxed over 5×10^5 steps and the mean square displacement $\Delta r_X(t)^2$ is examined. As observed in Figure 9, the diffusion coefficients of Al and O atoms decrease with increasing pressure. This is due to the bond Al–O in HD phase became much stronger than that in LD phase, resulting in a decrease in diffusion coefficients of Al and O in liquid Al_2O_3. According to Figure 9, there is the anomalous in the diffusion coefficient occurred at a pressure of 15 GPa for D_{Al}, and around 21 GPa for D_O, these values belonged the pressure range that the system is transforming from a tetrahedral to an octahedral network. This phenomenon may be related to breaking the Al-O links in the AlO_5 units. It resulted in the interaction between atoms in the AlO_5 units to weaken and molecular structure was more easily broken. Therefore, the structural transformation was also accompanied by anomalous diffusion. In addition, it is interesting to note that the basic units AlO_x are identical in different pressures as confirmed from Figures 4 and 5. As a result, the diffusion coefficients of X-atoms, D_X may be expressed through fraction of AlO_x units, it has form as follows

$$D_X = C_4D_{LD} + (C_5 + C_6 + C_7)D_{HD} \quad (7)$$

where C_4, C_5, C_6 and C_7 are the fraction of AlO_x (x = 4, 5, 6, 7), respectively, D_{LD} and D_{HD} are the diffusion coefficients in LD and HD phases. The D_{LD} and D_{HD} coefficients are calculated by fitting function in Eq. (6) with molecular dynamics simulation data. These fitting parameters are D_{HD} = 4.801×10^{-6}, 4.62×10^{-6} and D_{LD} =1.797×10^{-6}, 3.034×10^{-6} cm^2/s for Al and O atoms, respectively. Therefore, the coefficients of X-atoms in liquid may be calculated by Eq. (7), as the fraction of AlO_x units is determined.

IV. Conclusion

We successfully performed a simulation of glass and liquid Al_2O_3 with pressure ranging from 0 to 30 GPa, the temperature of 300 and 3000 K, which could provide experimental basic to develop ceramic materials with outstanding properties. We draw main conclusions as follows

i) The result shows that the structure origination of liquid and glass Al_2O_3 is built mainly by AlO_x (x = 3-7) units that are linked to each other via common O atoms. With increasing pressure, there is the transformation from tetrahedral to octahedral network structure, in which the phase transition pressure, as well as the phase transition pressure range in liquid, is lower (smaller) than ones in glass.

ii) According to the analysis of fraction of AlO_x basic units and snapshot of the positions of atoms, the distribution of AlO_x units in liquid is not uniform but tends to form AlO_x-clusters. The AlO_4-clusters form the LD-phase; in contrast, the AlO_5-, AlO_6-, and AlO_7-clusters form the HD-phase. Under compression, the liquid Al_2O_3 consists of separate LD- and HD- phases. The size of separate phases significantly depends on compression.

iii) With increasing pressure, the fraction of AlO_x units significantly varies, but partial bond angle and length distributions of AlO_x units are identical for all the different pressures. We found that a simple correlation between the density, diffusion coefficients and the characteristics of the two-phase model. As a result, our work supports a technique to determine the diffusion coefficients, as well as the density of oxide systems.

Acknowledgement

This research is funded by Thai Nguyen University and Thai Nguyên University of Education under grant number ĐH2023-TN04-04.

References

[1]. Bi, Zhisheng, et al. "Performance and transition mechanism from acidity to basicity of amphoteric oxides (Al_2O_3 and B_2O_3) in SiO_2–CaO–Al_2O_3–B_2O_3 system: A molecular dynamics study." *Ceramics International* 47.9 (2021): 12252-12260.

[2]. Deng, Binghui, Adama Tandia, and Ying Shi. "Impact of pressure on structure and properties of hot-compressed Na_2O–Al_2O_3–SiO_2 glass by molecular dynamics simulations." *Journal of the American Ceramic Society* 104.6 (2021): 2530-2538.

[3]. Yuan, Y. G., et al. "Ab initio molecular dynamics simulation of low energy radiation responses of α-Al_2O_3." *Scientific reports* 7.1 (2017): 1-11.

[4]. Gu, Shaopeng, et al. "Effect of Al_2O_3 on non-Newtonian property and its relation to structure of mold fluxes during shear stress field at 1573 K." *Journal of Non-Crystalline Solids* 547 (2020): 120312.

[5]. Li, Long, et al. "Stability, thermal performance and artificial neural network modeling of viscosity and thermal conductivity of Al_2O_3-ethylene glycol nanofluids." *Powder Technology* 363 (2020): 360-368.

[6]. Le, Chinh T., Trang T. Nguyen, Thao T. Nguyen, and Vinh V. Le. "Molecular dynamics simulation of phase transformation and mechanical behavior in Al_2O_3 model." *Vacuum* 167 (2019): 175-181.

[7]. Ha, N. T. T., N. V. Hong, and P. K. Hung. "Network structure and dynamics heterogeneities in Al_2O_3 system: insight from visualization and analysis of molecular dynamics data." *Indian Journal of Physics* 93, no. 8 (2019): 971-978.

[8]. Zhang, Lei, Wan-lin Wang, and Han-qing Shao. "Review of non-reactive CaO–Al_2O_3-based mold fluxes for casting high-aluminum steel." *Journal of Iron and Steel Research International* 26.4 (2019): 336.

[9]. Li, Zhirong, et al. "Dissolution behaviour of Al_2O_3 in mould fluxes with low SiO_2 content." *Ceramics International* 45.3 (2019): 4035-4042.

[10]. Wang, Zhanjun, and Il Sohn. "Effect of substituting CaO with BaO on the viscosity and structure of CaO-BaO-SiO_2-MgO- Al_2O_3 slags." *Journal of the American Ceramic Society* 101.9 (2018): 4285-4296.

[11]. Li, Renwei, et al. "Insight into diffusion-rebonding of Nano- Al_2O_3 on Fe surface in high-temperature thermal energy storage system." *Applied Surface Science* 530 (2020): 147249.

[12]. Verma, Ashok K., P. Modak, and Bijaya B. Karki. "First-principles simulations of thermodynamical and structural properties of liquid Al_2O_3 under pressure." *Physical Review B* 84, no. 17 (2011): 174116.

[13]. Ansell, Stuart, Shankar Krishnan, JK Richard Weber, John J. Felten, Paul C. Nordine, Mark A. Beno, David L. Price, and Marie-Louise Saboungi. "Structure of liquid aluminum oxide." *Physical Review Letters* 78, no. 3 (1997): 464.

[14]. Lamparter, P., and R. Kniep. "Structure of amorphous Al_2O_3." *Physica B: Condensed Matter* 234 (1997): 405-406.

[15]. Gutierrez, Gonzalo, and Börje Johansson. "Molecular dynamics study of structural properties of amorphous Al_2O_3." *Physical Review B* 65, no. 10 (2002): 104202.

[16]. Davis, Sergio, and Gonzalo Gutiérrez. "Structural, elastic, vibrational and electronic properties of amorphous Al_2O_3 from ab initio calculations." *Journal of Physics: Condensed Matter* 23, no. 49 (2011): 495401.

[17]. Hennet, Louis, Dominique Thiaudiere, Marc Gailhanou, Claude Landron, Jean-Pierre Coutures, and David L. Price. "Fast x-ray scattering measurements on molten alumina using a 120 curved position sensitive detector." *Review of scientific instruments* 73, no. 1 (2002): 124-129.

[18]. Vo, Van Hoang, and Suhk Kun Oh. "Simulation of structural properties and structural transformation of amorphous Al_2O_3." *Physica. B, Condensed Matter* 352, no. 1-4 (2004): 73-85.

[19]. Landron, C., L. Hennet, T. E. Jenkins, G. N. Greaves, J. P. Coutures, and A. K. Soper. "Liquid alumina: detailed atomic coordination determined from neutron diffraction data using empirical potential structure refinement." *Physical review letters* 86, no. 21 (2001): 4839.

[20]. Waseda, Y., K. Sugiyama, and J. M. Toguri. "Direct determination of the local structure in molten alumina by high temperature X-ray diffraction." *Zeitschrift für Naturforschung A* 50, no. 8 (1995): 770-774.

[21]. Skinner, Lawrie B., Adrian C. Barnes, Philip S. Salmon, Louis Hennet, Henry E. Fischer, Chris J. Benmore, Shinji Kohara et al. "Joint diffraction and modeling approach to the structure of liquid alumina." *Physical Review B* 87, no. 2 (2013): 024201.

[22]. Wilding, Martin C., Mark Wilson, and Paul F. McMillan. "Structural studies and polymorphism in amorphous solids and liquids at high pressure." *Chemical Society Reviews* 35, no. 10 (2006): 964-986.

[23]. McMillan, Paul F., Mark Wilson, Martin C. Wilding, Dominik Daisenberger, Mohamed Mezouar, and G. Neville Greaves. "Polyamorphism and liquid–liquid phase transitions: challenges for experiment and theory." *Journal of Physics: Condensed Matter* 19, no. 41 (2007): 415101.

[24]. Karki, Bijaya B., Dipesh Bhattarai, and Lars Stixrude. "First-principles simulations of liquid silica: Structural and dynamical behavior at high pressure." *Physical Review B* 76, no. 10 (2007): 104205.

[25]. Jiang, Chunhe, et al. "Effect of MgO/Al_2O_3 ratio on the structure and properties of blast furnace slags: A molecular dynamics simulation." *Journal of Non-Crystalline Solids* 502 (2018): 76-82.

[26]. Guo, Hui, et al. "Study on micro-structure and transport properties of KF-NaF-AlF_3- Al_2O_3 system by first-principles molecular dynamics simulation." *Journal of Fluorine Chemistry* 235 (2020): 109546.

[27]. Gao, Longfei, et al. "Structure and flow properties of coal ash slag using ring statistics and molecular dynamics simulation: Role of CaO/Na_2O in SiO_2– Al_2O_3–CaO–Na_2O." *Chemical Engineering Science* 231 (2021): 116285.
[28]. Feng, Yuan, et al. "First-Principles Molecular Dynamics Simulation on High Silica Content Na_3AlF_6– Al_2O_3–SiO_2 Molten Salt." *ACS omega* 6.5 (2021): 3745-3751.
[29]. Vogel, Michael, and Sharon C. Glotzer. "Spatially heterogeneous dynamics and dynamic facilitation in a model of viscous silica." *Physical review letters* 92, no. 25 (2004): 255901.
[30]. Mizuno, Hideyuki, and Ryoichi Yamamoto. "Dynamical heterogeneity in a highly supercooled liquid: Consistent calculations of correlation length, intensity, and lifetime." *Physical Review E* 84, no. 1 (2011): 011506.
[31]. Gutiérrez, Gonzalo, et al. "Structural properties of liquid Al_2O_3: A molecular dynamics study." *Physical review E* 61.3 (2000): 2723.
[32]. Vashishta, Priya, et al. "Interaction potentials for alumina and molecular dynamics simulations of amorphous and liquid alumina." *Journal of Applied Physics* 103.8 (2008): 083504.
[33]. Libor Kovarik, Mark Bowden, János Szanyi. "High temperature transition aluminas in d- Al_2O_3 /h- Al_2O_3 stability range: Review." *Journal of Catalysis* 393 (2021) 357–368.
[34]. Lascaris, Erik, Mahin Hemmati, Sergey V. Buldyrev, H. Eugene Stanley, and C. Austen Angell. "Diffusivity and short-time dynamics in two models of silica." *The Journal of chemical physics* 142, no. 10 (2015): 104506.
[35]. Daisenberger, Dominik, Mark Wilson, Paul F. McMillan, Raul Quesada Cabrera, Martin C. Wilding, and Denis Machon. "High-pressure x-ray scattering and computer simulation studies of density-induced polyamorphism in silicon." *Physical Review B* 75, no. 22 (2007): 224118.
[36]. Morishita, Tetsuya. "High density amorphous form and polyamorphic transformations of silicon." *Physical review letters* 93, no. 5 (2004): 055503.
[37]. Lelong, G., L. Cormier, G. Ferlat, V. Giordano, G. S. Henderson, A. Shukla, and G. Calas. "Evidence of fivefold-coordinated Ge atoms in amorphous GeO_2 under pressure using inelastic x-ray scattering." *Physical Review B* 85, no. 13 (2012): 134202.
[38]. Van Hoang, Vo, Nguyen Huynh Tuan Anh, and Hoang Zung. "Liquid–liquid phase transition and anomalous diffusion in simulated liquid GeO_2." *Physica B: Condensed Matter* 390, no. 1-2 (2007): 17-22.
[39]. Saika-Voivod, Ivan, Francesco Sciortino, Tor Grande, and Peter H. Poole. "Phase diagram of silica from computer simulation." *Physical Review E* 70, no. 6 (2004): 061507.
[40]. Richet, Pascal, Grant S. Henderson, and Daniel R. Neuville. "Thermodynamics: The oldest branch of Earth sciences?." *Elements* 6, no. 5 (2010): 287-292.
[41]. Koziatek, P., J. L. Barrat, and D. Rodney. "Short-and medium-range orders in as-quenched and deformed SiO_2 glasses: An atomistic study." *Journal of Non-Crystalline Solids* 414 (2015): 7-15.

Table 1. The structural characteristics of constructed models at different pressures, experimental and simulation data: $r_{X\text{-}Y}$ - the inter-atomic distance for X-Y pair; $Z_{X\text{-}Y}$ - the average coordination number for X-Y; θ - position of the highest peak of BAD.

Models	0	5	10	15	20	25	30		
	Al_2O_3 glass (Temperature of 300 K)							Simu. [15]	Exp. [14]
$r_{Al\text{-}Al}$ (Å)	3.14	3.1	3.06	3.04	3.02	3.02	2.98	3.12±0.25	3.2±0.55
$r_{Al\text{-}O}$ (Å)	1.74	1.72	1.72	1.72	1.72	1.74	1.74	1.76±0.1	2.8±0.58
$r_{O\text{-}O}$ (Å)	2.8	2.78	2.74	2.68	2.64	2.6	2.6	2.75±0.2	1.8±0.21
$Z_{Al\text{-}Al}$	7.92	8.15	8.86	9.78	10.32	11.16	11.37	8.26	8.26
$Z_{Al\text{-}O}$	4.3	4.35	4.54	4.72	4.9	5.13	5.2	4.25	4.25
$Z_{O\text{-}Al}$	2.86	2.9	3.03	3.15	3.26	3.42	3.47	2.83	-
$Z_{O\text{-}O}$	11.8	12.18	13.15	14.11	14.83	15.6	15.86	9.47	9.47
$\theta_{O\text{-}Al\text{-}O}$	90°; 119°	90°; 119°	89°; 119°	89°; 118°	89°; 118°	88°; 118°	87°; 117°	90°; 120°	
$\theta_{Al\text{-}O\text{-}O}$	105°	105°	105°	105°	105°	105°	105°	105°	
	Al_2O_3 liquid (Temperature of 3000 K)							Simu. [31]	Exp. [19]
$r_{Al\text{-}Al}$ (Å)	3.1	3.14	3.08	3.06	3.02	3.04	3	3.15±0.4	3.25
$r_{Al\text{-}O}$ (Å)	1.68	1.7	1.7	1.7	1.72	1.72	1.74	1.75	1.78
$r_{O\text{-}O}$ (Å)	2.76	2.74	2.68	2.66	2.6	2.56	2.56	2.75	2.84
$Z_{Al\text{-}Al}$	7.9	9.15	9.91	10.51	11.3	11.61	11.89	8.24	-
$Z_{Al\text{-}O}$	4.21	4.5	4.68	4.84	5.1	5.22	5.34	4.1	4.20
$Z_{O\text{-}Al}$	2.81	3	3.12	3.22	3.4	3.48	3.56	2.72	-
$Z_{O\text{-}O}$	11.77	13.25	14.06	14.69	15.37	15.74	16.03	8.84	-
$\theta_{O\text{-}Al\text{-}O}$	95°	95°	94°	93°	93°	91°	90°	95°	-
$\theta_{Al\text{-}O\text{-}Al}$	115°	115°	114°	114°	113°	114°	113°	115°	-

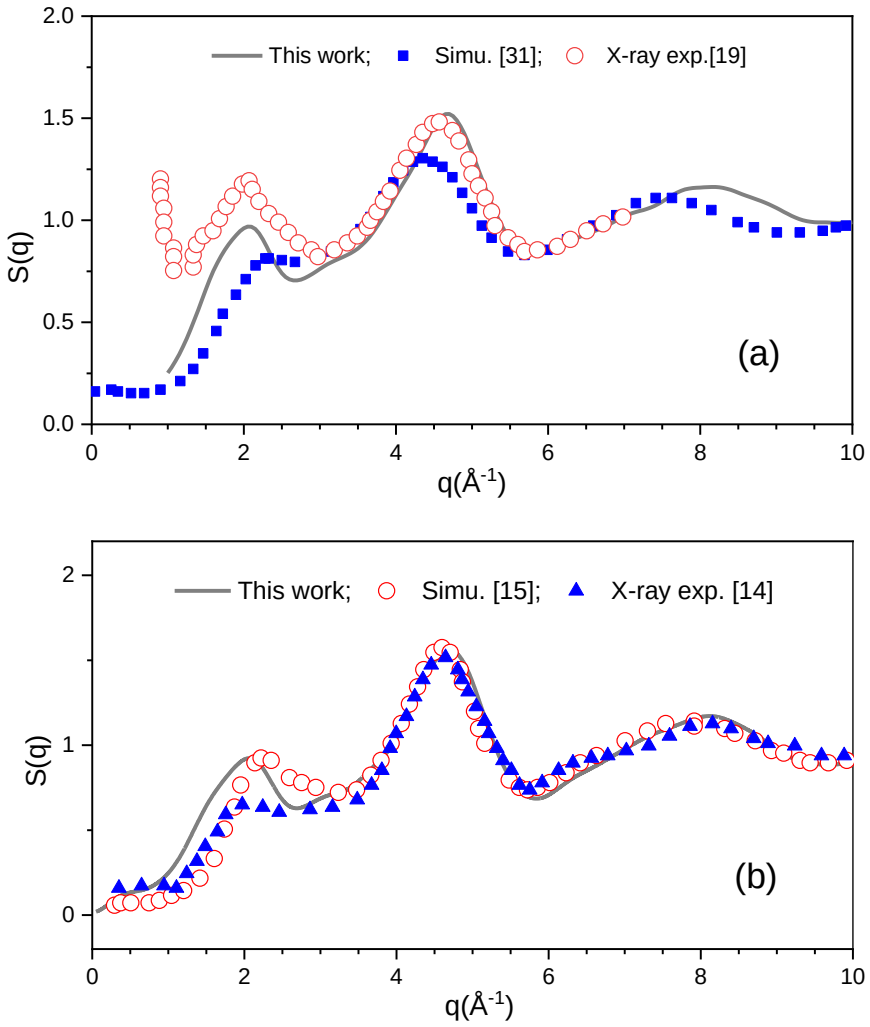

FIG 1. The comparison between the X-ray experimental structure factors and those calculated from the simulation model for liquid (a) and glass (b) Al_2O_3; Red open symbol is experimental results of Lamparter et al., and Landron et al.; blue solid symbol is simulation results of Gutierrez et al.; the solid line gives the simulation results.

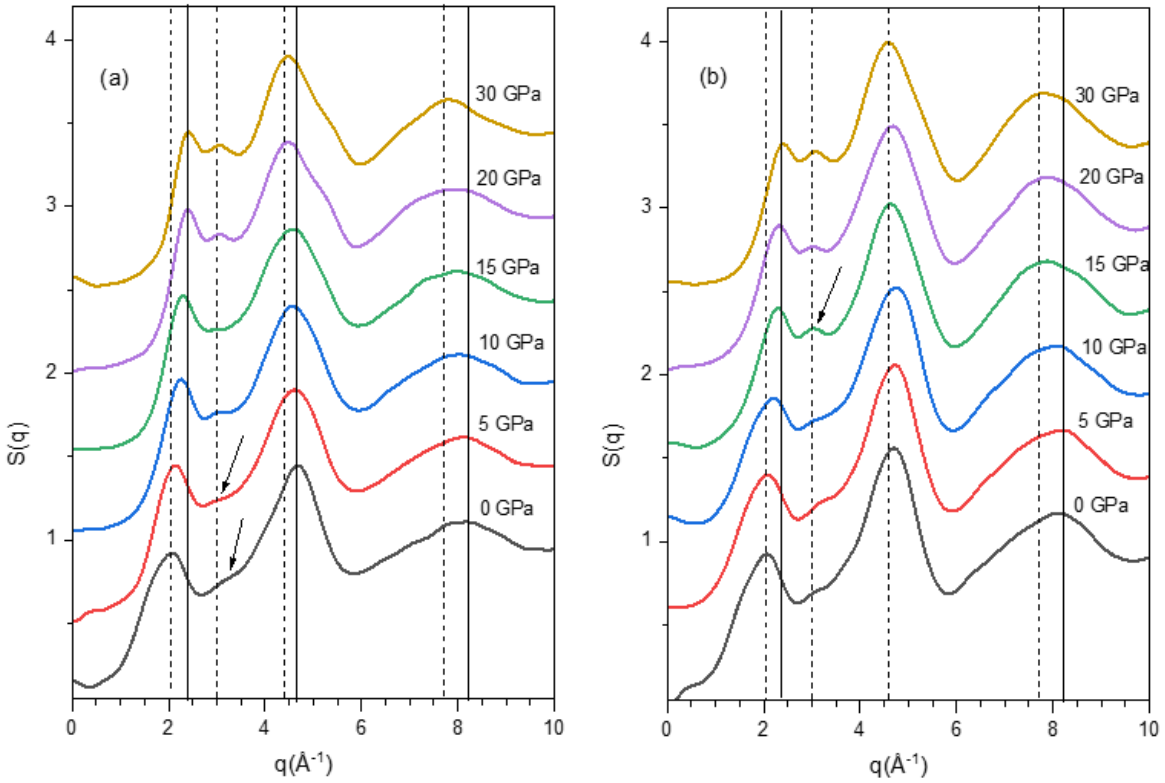

FIG. 2. The total X-ray scattering structure factors of Al2O3 liquid (a) and glasses (b) at different pressures; the black arrows denote the phase transition points; the solid and dotted line presents the shift distances of the peak position.

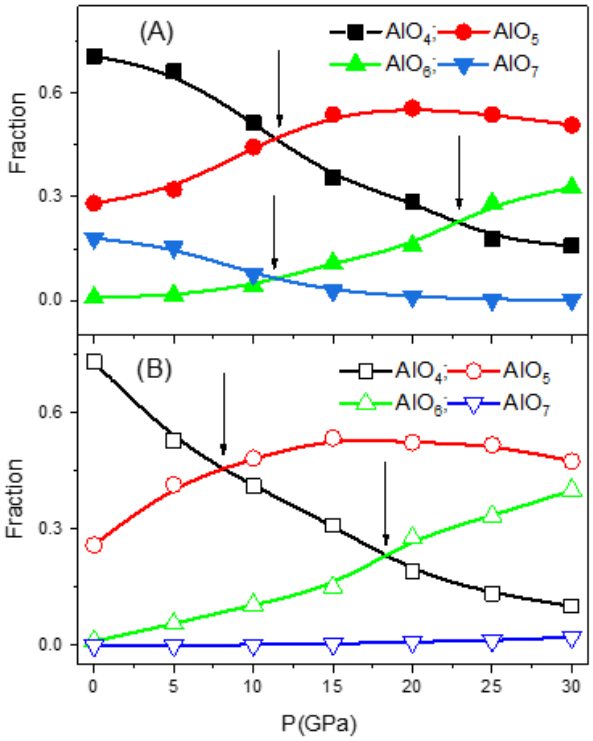

FIG. 3. The pressure dependence of fraction of basic units; A and B panel show the fraction of CAlO4, CAlO5, CAlO6 and CAlO7 for Al2O3 liquid and glass, respectively.

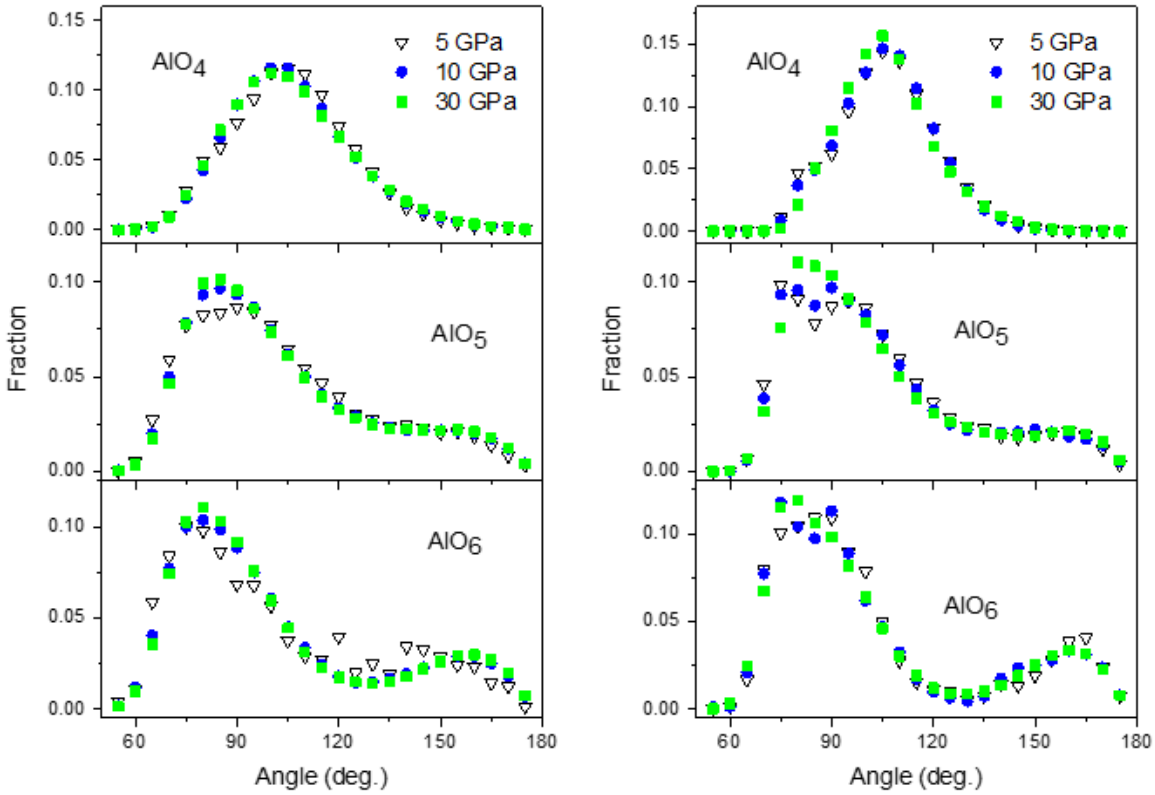

FIG. 4. The bond angle distribution in AlO4, AlO5 and AlO6 units for Al2O3 liquid (left) and glass (right) at pressures of 5, 10 and 30 GPa.

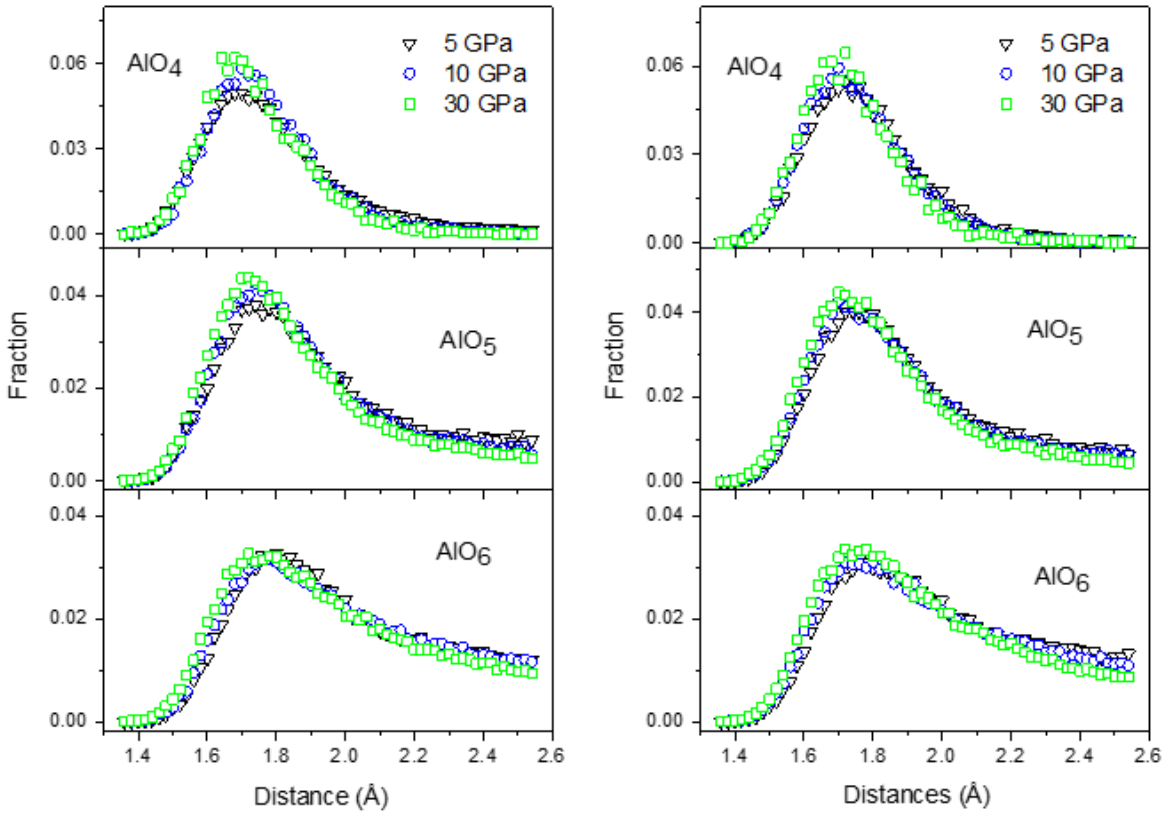

FIG. 5. The bond length distribution in AlO4, AlO5 and AlO6 units for Al2O3 liquid (left) and glass (right) at pressures of 5, 10 and 30 GPa.

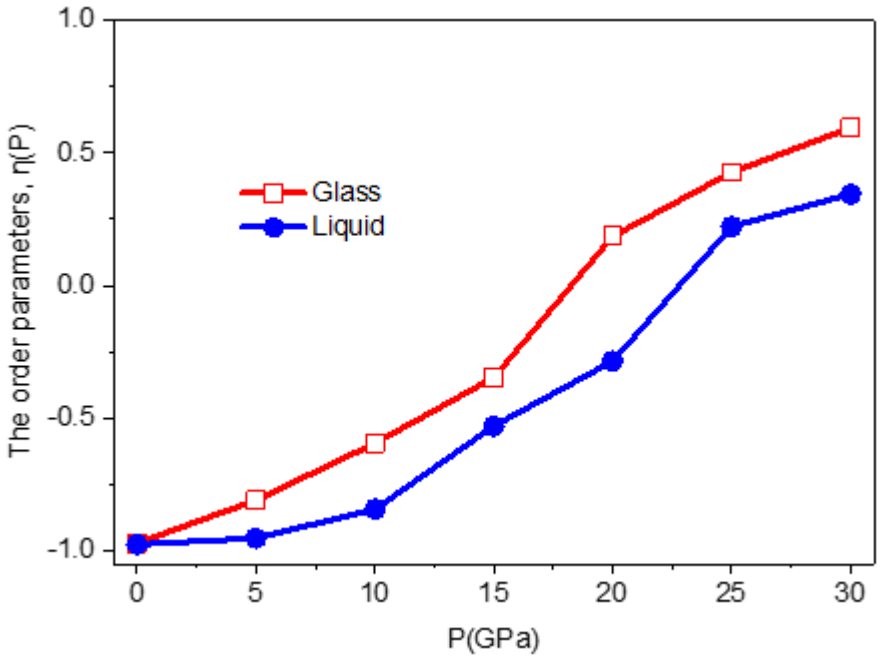

FIG. 6. The pressure dependence of the order parameter, η for Al2O3 for Al2O3 liquid and glass

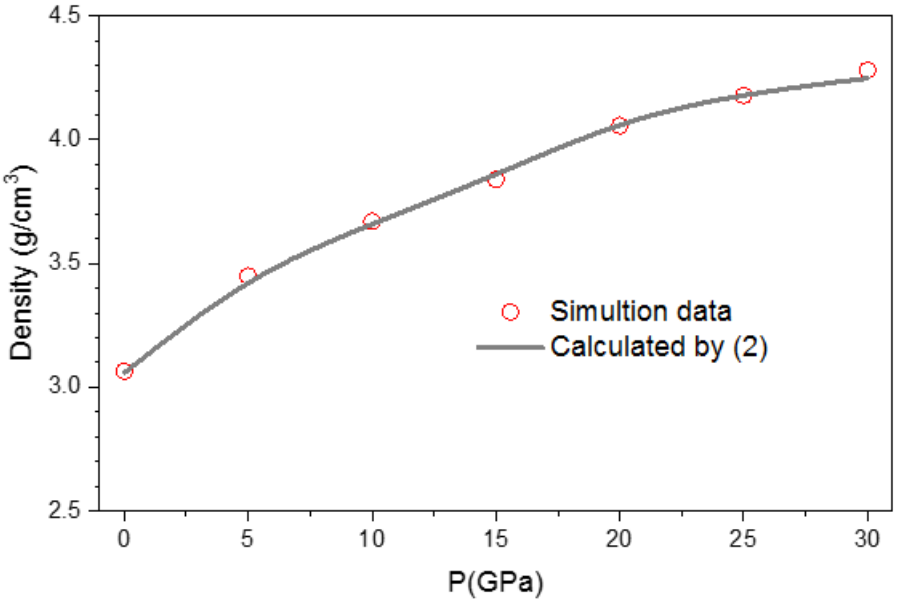

FIG. 7. The pressure dependence of density of liquid Al_2O_3

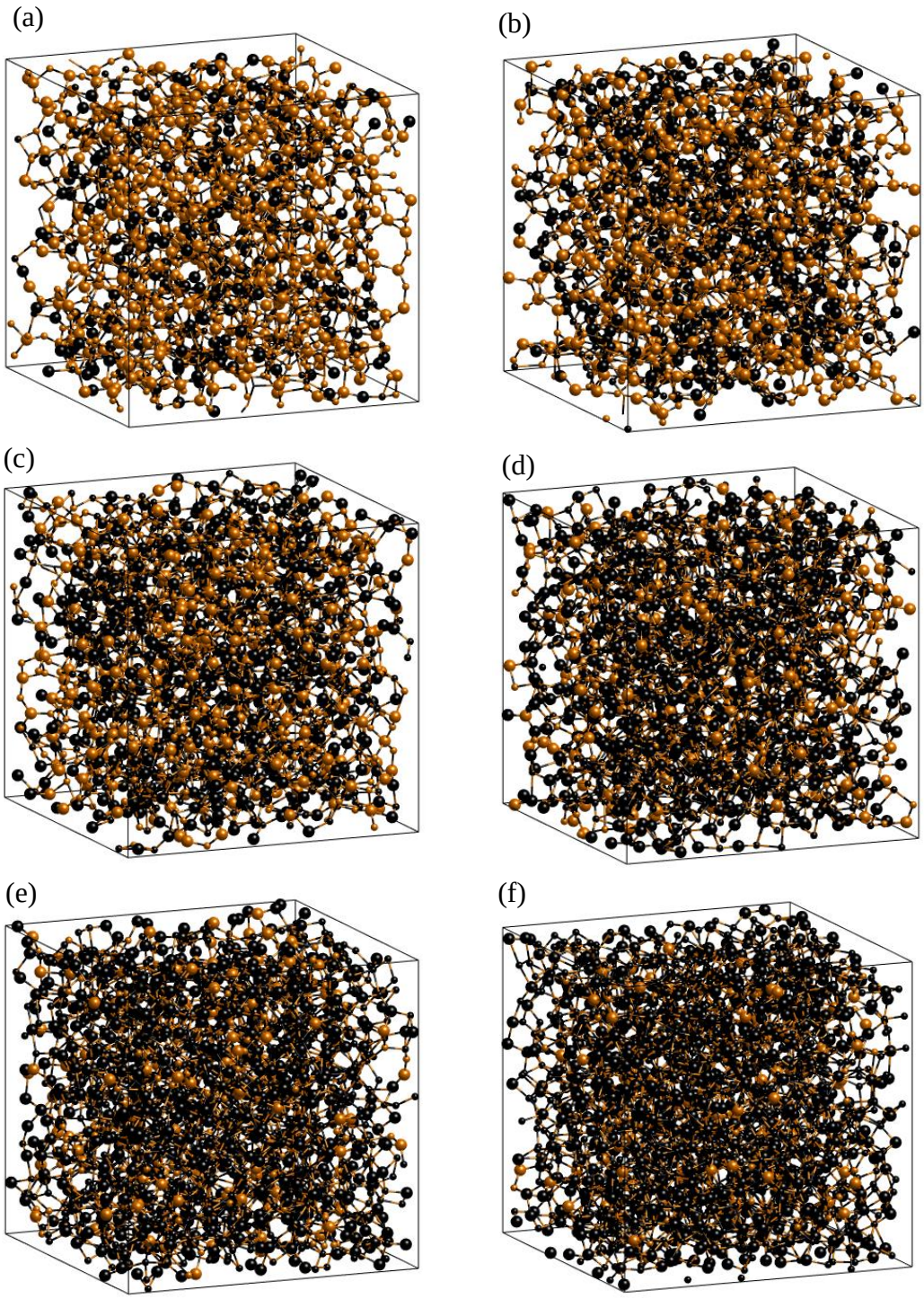

FIG. 8. Snapshot of the positions of atoms in LD-phase (AlO_4 units) and HD-phase (AlO_5, AlO_6 units of Al_2O_3 model at 0 GPa (a), 5 GPa (b), 10 GPa (c), 15 GPa (d), 20 GPa (e) and 30 GPa (f). Region with yellow color is a cluster of AlO_4, black color is cluster of AlO_5, AlO_6 and AlO_7 units. The big sphere is O atom; the small sphere is Al atom.

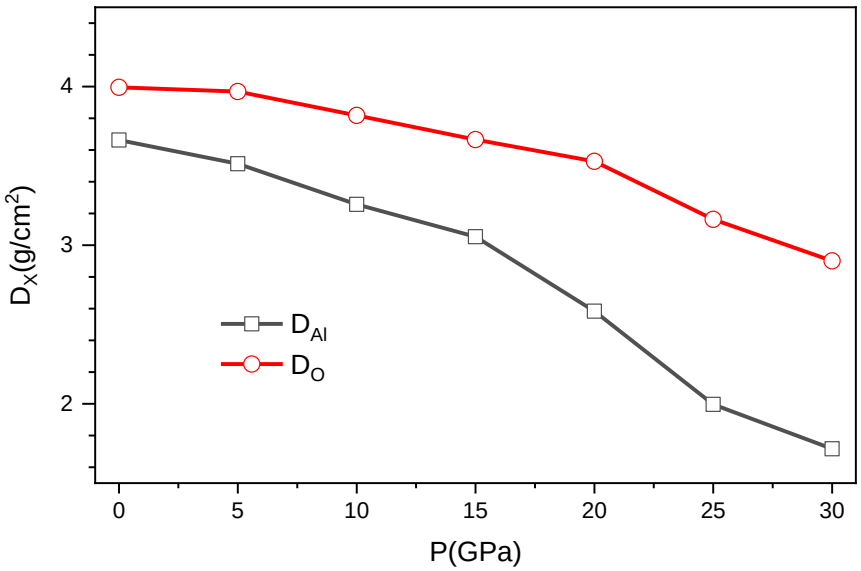

FIG. 9. The pressure dependence of the diffusion coefficient in liquid Al_2O_3